Hierarchical mesoporous $SrCO_3$ submicron spheres derived from reaction-limited aggregation induced "rod-to-dumbbell-to-sphere" self-assembly†

Wancheng Zhu,*[a] Guanglei Zhang,[a] Jing Li,[a] Qiang Zhang,‡[b] Xianglan Piao[b] and Shenlin Zhu[b]

Received 4th November 2009, Accepted 17th December 2009
First published as an Advance Article on the web 23rd January 2010
DOI: 10.1039/b923169b

Hierarchical mesoporous $SrCO_3$ submicron spheres were fabricated *via* a facile and direct hydrothermal method. This was realized *via* the room temperature co-precipitation of Na_2CO_3 and $SrCl_2$ solution in presence of appropriate amount of $MgCl_2$ and ethylene diamine tetraacetic acid disodium salt, which led to bouquet-like $SrCO_3$ nanostructures at first. Then the precipitate was hydrothermally treated at 190 °C for 12.0 h, resulting in uniform hierarchical $SrCO_3$ submicron spheres. The characterization results definitely determined the hierarchical $SrCO_3$ submicron spheres of mesoporous structure, bearing a specific surface area of 40.2 $m^2\ g^{-1}$, a total pore volume of 0.145 $cm^3\ g^{-1}$, and a narrow pore size distribution concentrating on 3–20 nm with an average pore diameter of 14.4 nm. Finally, the reaction-limited aggregation induced "rod-to-dumbbell-to-sphere" mechanism was proposed to explain the formation of the hierarchical mesoporous submicron spheres.

1. Introduction

Controlling the initial growth and further assemblies of the building blocks, at micro- and nanoscale level, into target structured materials bearing the controlled size and tailored morphology has become one of the most important aspects in the modern synthesis.[1,2] Recently, complex architectures, especially three-dimensional hierarchical architectures assembled by one-dimensional (1D) nanostructures[3,4] have attracted extraordinary attention and intensive interests due to their unique structures and fantastic properties different from those of the monomorph structures.[5,6] The hierarchical structures, or superstructures, are expected to play a significant role in fabricating the next generation of microelectronic and optoelectronic devices for their potential applications as both building units and interconnections.[7] Particularly, hierarchical architectures with porous structures have triggered more and more research enthusiasm in recent years for their high surface-to-volume ratio and permeability, and synthesis of mesoporous materials has become a remarkable level in modern materials chemistry.[6,8]

As a matter of fact, mesoporous materials have been extensively explored since the discovery of M41S family in 1992,[8,9] owing to their great potentials as candidates wide used in catalysis,[10] optics,[11] photonics, sensors, separation, drug delivery,[12] sorption,[13] acoustic or electrical insulation, and ultra-light structural materials,[14–16] *etc.* Mesoporous materials are generally synthesized *via* a soft or hard template aided process, which usually however, suffers from the removal of templates and resultant structural collapse[17] although hydrothermal synthesis and hydrothermal treatment have been extensively investigated either in preparation[6,18,19] or in post-treatment[20,21] with the attempt to improve the corresponding hydrothermal stability[22–25] of the as-synthesized mesoporous materials. Consequently, great efforts have been made to directly grow mesoporous inorganic materials in absence of any templates in recent years.[26] On the other hand, as one of the most efficient methods of soft chemistry, hydrothermal technologies have been widely employed in the process of 1D nanostructues[27] because of the distinct advantages over other traditional methods.[28] Most recently, hydrothermal method has also been emerged as a thriving technique for the facile fabrication of the complex hierarchical architectures, such as cantaloupe-like AlOOH superstructures,[29a] $Co(OH)_2$ and Co_3O_4 nanocolumns,[29b] $NdOHCO_3$ dendrites,[29c] ZnSe nanoflowers,[29d] flower-like and well-aligned nanorod hierarchical CeO_2 architectures,[29e] hierarchical microspheres of Bi_2WO_6,[29f] $Ni(OH)_2$ and NiO,[29g] and even hierarchical mesoporous microspheres of $InVO_4$.[6]

Strontium carbonate ($SrCO_3$) is an important reagent and has traditionally been used as an additive in the production of iridescent and speciality glasses, pigments, driers, paints, pyrotechnics, strontium metal and other strontium compounds,[30] and also utilized as the constituent of ferrite magnets for small direct current motors and as an additive in the manufacture of glass for color television tubes.[31] Recently, novel applications of $SrCO_3$ have also been reported, including $SrCO_3$-based chemiluminescence sensors exhibiting high selectivity to ethanol,[32a] $Co/SrCO_3$ catalyst displaying high activity for dry reforming of methane with small amount of carbon deposition,[32b] and $SrCO_3$ catalyst for ethanol degradation.[32c] Correspondingly, various morphologies of $SrCO_3$ nanostructures, such as nanoparticles,[32a]

[a]*Department of Chemical Engineering, Qufu Normal University, Shandong, 273165, China. E-mail: zhuwancheng@tsinghua.org.cn; Fax: +86-537-4456305*
[b]*Department of Chemical Engineering, Tsinghua University, Beijing, 100084, China*

† Electronic supplementary information (ESI) available: The variation of the crystallinity, precipitate and precipitate yield of the hydrothermal product with the hydrothermal temperature (Fig. S1), size distribution of the hierarchical mesoporous $SrCO_3$ submicron spheres (Fig. S2), and effect of the additives on the morphology of the hydrothermally treated $SrCO_3$ particles (Fig. S3). See DOI: 10.1039/b923169b

‡ Present address: Department of Chemical Engineering, Case Western Reserve University, Cleveland, OH 44106, USA.

nanowhiskers,[33a] nanowires,[33b] and nanoneedles,[33c] and also microstructures, with needle-like,[34a–b] fusiform prism-like,[34c] rod-like, whisker-like, and ellipsoid-like[35] shape, have been obtained. Very recently, $SrCO_3$ architectures assembled by prime nanoparticles or 1D nanostructures, such as flower-like,[36a–b] bundle-like, dumbbell-like, hexagonal star-like,[37a–b] branch-like,[37c] especially spherical or sphere-like[33a,35,37a–b] $SrCO_3$ microstructures have also been acquired. $SrCO_3$ microspheres could be formed by enzyme-catalyzed decomposition of urea in aqueous solutions of strontium salts at room temperature,[33a] and room temperature aging method in presence of appropriate additives, such as poly-(styrene-alt-maleic acid) (PSMA)[37a] and ethylene diamine tetraacetic acid (EDTA),[37b] as well as microemulsion-mediated solvothermal synthesis in presence of cetyltrimethylammonium bromide (CTAB).[35] Du *et al.* reported the synthesis of mesoporous $SrCO_3$ spheres in the previously prepared room temperature ionic liquid (ILs) 1,1,3,3-tetramethylguanidinium lactate.[38] Most recently, Wang *et al.* reported the hierarchical $SrCO_3$ architectures synthesized by room temperature aging method (5 days) based on the conversion of pre-synthesized $SrCrO_4$ nanowires.[39] To date, it is still a great challenge to facilely and directly synthesize hierarchical mesoporous $SrCO_3$ architectures.

In this work, we report for the first time, to the best of our knowledge, a facile and direct hydrothermal method (190 °C, 12.0 h) for hierarchical mesoporous $SrCO_3$ submicron spheres in presence of appropriate amount of EDTA disodium salt and $MgCl_2$, taking strontium chloride hexahydrate ($SrCl_2 \cdot 6H_2O$) and sodium carbonate anhydrous (Na_2CO_3) as the starting materials. Based on the experimental results, a reaction-limited aggregation (RLA) induced "rod-to-dumbbell-to-sphere" self-assembly mechanism was proposed. The hierarchical mesoporous $SrCO_3$ submicron spheres may be expected in the hierarchical mesoporous materials family for the narrow pore size distribution with a relatively large average pore diameter, a probable high hydrothermal stability and great potential applications, and the developed facile RLA induced "rod-to-dumbbell-to-sphere" self-assembly mechanism may also be extended to the preparation of other carbonates and non-silica hierarchical mesostructured materials.

2. Experimental

Synthesis

$SrCO_3$ submicron spheres were synthesized *via* a co-precipitation of $SrCl_2$ and Na_2CO_3 solution at room temperature followed by a facile hydrothermal treatment of the slurry at 190 °C for 12.0 h in presence of appropriate amount of $MgCl_2$ and EDTA disodium salt as additives, all reagents including $SrCl_2 \cdot 6H_2O$ and Na_2CO_3 were analytical grade and used directly without further purification. In a typical procedure, 10 mL of Na_2CO_3 solution (1.41 mol L^{-1}) was dropped into 11 mL of $SrCl_2$ solution (1.41 mol L^{-1}) under vigorous magnetic stirring at room temperature (dropping rate: 1 droplet per second approx.), leading to a white slurry. 0.4187 g of EDTA disodium salt and 0.1398 g of $MgCl_2 \cdot 6H_2O$ (keeping molar ratios of EDTA and $MgCl_2$ to Na_2CO_3 as 5%) were added into the previously resultant and continuously stirred slurry, which was supplied deionized (DI) water to 55 mL and kept stirring for another 3 min and finally transferred into a Teflon-lined stainless steel autoclave with a capacity of 70 mL. The autoclave was sealed and heated (1 °C min^{-1}) to 190 °C and kept in an isothermal state for 12.0 h and then cooled down to room temperature naturally. The precipitate was filtered, washed with DI water and absolute alcohol for three times, respectively, and finally dried at 120 °C for 6.0 h for further characterization. To investigate the effects of the reactants and additives on the morphologies of the hydrothermally treated product, molar ratio of $SrCl_2$ to Na_2CO_3, EDTA disodium salt to Na_2CO_3, and also $MgCl_2$ to Na_2CO_3 were adjusted within the range of 1.05 : 1–1 : 2.0, 0 : 100–5 : 100, 0 : 100–5 : 100, respectively, with other conditions kept the same. To understand the hydrothermal formation of the mesoporous $SrCO_3$ submicron spheres, the hydrothermal product acquired from the precipitate heated to various designated temperature moments within the range of 80–190 °C were collected instead of being kept under isothermal conditions for some time.

Characterization

The crystal phase and structure of the sample were identified by the X-ray powder diffractometer (XRD, D/MAX 2500, Rigaku, Japan) using a Cu Kα radiation (λ = 1.54178 Å) and a fixed power source (40.0 kV, 200.0 mA). The morphology, microstructure and composition of the samples were examined by the field emission scanning electron microscopy (FESEM, JSM 7401F, JEOL, Japan) operated at an accelerating voltage of 3.0 kV, and a high resolution transmission electron microscopy (HRTEM, JEM-2010, JEOL, Japan) performed at an accelerating voltage of 120.0 kV equipped with an X-ray energy dispersive spectrometer (EDS, INCA Energy TEM, Oxford Instruments, UK) and a charge coupled device (CCD) camera (Orius SC 1000, Gatan, USA). To minimize the influence of the carbon element from the ordinary carbon film on the EDS spectrum of the sample, the sample was first dispersed in ethanol by ultrasonic treatment for 15 min and then deposited onto the holey carbon film supported by a copper grid. The size distribution of the as-synthesized submicron spheres was estimated by direct measuring about 200 particles from the typical FESEM images. The N_2 adsorption–desorption isotherms were measured at 77 K using a Chemisorption-Physisorption Analyzer (Autosorb-1-C, Quantachrome, USA) after the samples had been outgassed at 300 °C for 60 min. The specific surface area was calculated from the adsorption branches in the relative pressure range of 0.10–0.31 using multi-point Brunauer–Emmett–Teller (BET) method, and the pore size distribution was evaluated from the N_2 desorption isotherm using the Barrett–Joyner–Halenda (BJH) method.

3. Results and discussion

3.1 Hydrothermal formation of hierarchical $SrCO_3$ submicron spheres

$MgCl_2$ and EDTA disodium salt were both selected as the additives for the synthesis of $SrCO_3$ spheres, and the amount of $SrCl_2$ was kept relatively excessive corresponding to that of Na_2CO_3, so as to avoid introducing unwanted impurity of $MgCO_3$ although the solubility product constant (K_{sp}(25 °C))

of $SrCO_3$ (5.6×10^{-10}) is much smaller than that of $MgCO_3$ (6.82×10^{-6}). Effects of the additives and hydrothermal treatment on the composition and morphology of the product are shown in Fig. 1. The existence of additives do not influence the composition of the product, all samples were composed of orthorhombic $SrCO_3$ (strontianite, PDF# 05-0418), as shown by Fig. 1 (a–c). Dropping Na_2CO_3 into $SrCl_2$ (molar ratio, $SrCl_2 : Na_2CO_3 = 1.1 : 1$) in absence of any additives led to the white precipitate comprised of high-crystallinity (Fig. 1(a)), rough bouquet-like $SrCO_3$ nanostructures containing 1D assemblies from small nanoparticles coalesced in a head to head attached manner (Fig. 1(a_1)) at room temperature, similar to the branch-like $SrCO_3$ nanostructures formed by the microwave assisted synthesis in presence of ethylenediamine (EDA) additive.[37c] In contrast, the co-existence of $MgCl_2$ and EDTA disodium salt (molar ratio, additive : Na_2CO_3 = 5 : 100) promoted the formation of bouquet-like $SrCO_3$ architectures consisted of 1D nanostructures with a relatively high crystallinity (Fig. 1(b)) and smooth surface (Fig. 1(b_1)) at room temperature, analogous to the bundle-like $SrCO_3$ prepared under room temperature aging conditions, either with the same reactants whereas in presence of aminoacetic acid (Gly) (aging, 12 h)[37b] or with $Sr(NO_3)_2$ and Na_2CO_3 as the reactants in absence of PSMA (aging, 24 h),[37a] and also like the hydrothermally synthesized flower-like $SrCO_3$ nanostructures under 200 °C for 20 h without any additives.[36a] Interestingly, corresponded with the precipitate obtained in absence (Fig. 1(a,a_1)) or presence (Fig. 1(b,b_1)) of additives at room temperature, the hydrothermal treatment of the formerly acquired bouquet-like $SrCO_3$ architectures at 190 °C for 12.0 h resulted in hierarchical $SrCO_3$ submicron spheres (Fig. 1(c_1)) of ordinary crystallinity (Fig. 1(c)), somewhat like the spherical $SrCO_3$ reported in the literature by other methods,[33a,35,37a–b] and quite similar to the mesoporous $SrCO_3$ spheres obtained in room temperature ILs[38] and even hydrothermally synthesized mesoporous $InVO_4$ hierarchical microspheres.[6]

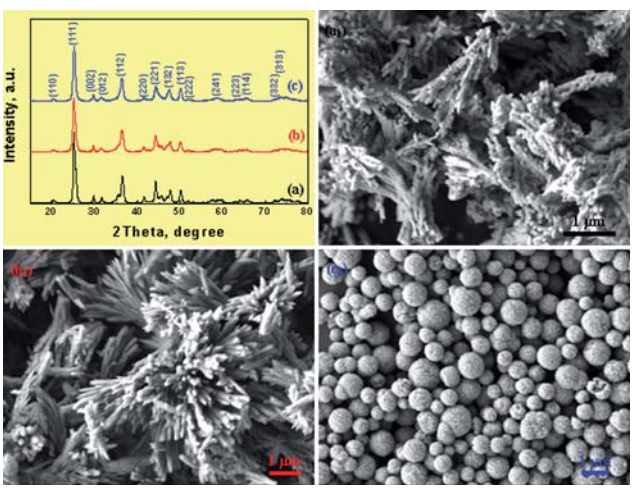

Fig. 1 XRD patterns (a–c) and SEM images (a_1–c_1) of the product obtained by dropping Na_2CO_3 into $SrCl_2$ (molar ratio, $SrCl_2 : Na_2CO_3 = 1.1 : 1$) in absence (a, a_1) or presence (b, b_1) of $MgCl_2$ and EDTA disodium salt as additives (molar ratio, additive : $Na_2CO_3 = 5 : 100$) at room temperature, or by the hydrothermal treatment of the precursor containing the former product (b, b_1) at 190 °C for 12.0 h (c, c_1).

Thus the formation of hierarchical $SrCO_3$ submicron spheres could be expressed as follows: co-precipitation of Na_2CO_3 and $SrCl_2$ in absence of additives at room temperature:

$$SrCl_2\ (aq) + Na_2CO_3\ (aq) \rightarrow SrCO_3\ (s, \text{rough bouquet-like}) + 2NaCl\ (aq). \quad (1)$$

Co-precipitation of Na_2CO_3 and $SrCl_2$ in presence of additives at room temperature:

$$SrCl_2\ (aq) + Na_2CO_3\ (aq) \rightarrow SrCO_3\ (s, \text{smooth bouquet-like}) + 2NaCl\ (aq). \quad (2)$$

Hydrothermal treatment of the precipitate at 190 °C for 12.0 h in presence of additives:

$$SrCO_3\ (s, \text{smooth bouquet-like}) \rightarrow SrCO_3\ (s, \text{hierarchical submicron spheres}). \quad (3)$$

Practically, the hydrothermal temperature has a slight influence on the crystallinity and significant impact on the precipitate and precipitate yield (ESI, Fig. S1).† The crystallinity of the hydrothermally treated $SrCO_3$ precipitate got higher with the increase in the temperature from 180 °C to 210 °C (Fig. S1(a)).† On the other hand, under the specific conditions (hydrothermal time (h): 12.0; molar ratio: EDTA disodium salt : Na_2CO_3 = 5 : 100, $MgCl_2 : Na_2CO_3 = 5 : 100$, $SrCl_2 : Na_2CO_3 = 1 : 2.01$.), with temperature increased within the range of 180–210 °C, the precipitate and precipitate yield increased up from 1.78 g to 1.84 g and dropped down to 1.81 g and finally to 1.80 g, from 89.8% to 93.2% and dropped down to 91.4% and finally to 91.1%, respectively (Fig. S1(b)).† Consequently, the hydrothermal treatment hereafter was performed at 190 °C. Meanwhile, the amount of $SrCl_2$ was strictly kept relatively excessive corresponding to that of Na_2CO_3 to avoid the introduction of the impurity $MgCO_3$ by the possible side reaction between Na_2CO_3 and $MgCl_2$.

3.2 Key influencing factors and synergistic effect of additives

Fig. 2 shows the influences of the molar ratio of $MgCl_2$ and $SrCl_2$ to Na_2CO_3 on the morphologies of the hydrothermally treated submicron $SrCO_3$ spheres obtained at 190 °C for 12.0 h, with the molar ratio of EDTA disodium salt to Na_2CO_3 as 5 : 100. Under the circumstances that $MgCl_2 : Na_2CO_3$ = 2.5 : 100 and $SrCl_2 : Na_2CO_3 = 1.05 : 1$, submicron $SrCO_3$ spheres with some detectable caves, interspaces and multitudinal nanoparticles attached on the surface were formed (Fig. 2(a,a_1)). Increasing $MgCl_2 : Na_2CO_3$ to 5 : 100 and keeping $SrCl_2 : Na_2CO_3$ as 1.05 : 1, submicron $SrCO_3$ spheres with a relatively wide distribution of the diameter whereas without distinct nanoparticles attached on the surface were obtained (Fig. 2(b)). Meanwhile, some submicron spheres assembled by various parts and even containing distinct caves on the surface were also existed (Fig. 2(b_1)), quite like the pitted whitethorn's fruit, indicating the assembled or aggregated growth phenomena of the $SrCO_3$ spheres. Keeping $MgCl_2 : Na_2CO_3$ as 5 : 100 and increasing $SrCl_2 : Na_2CO_3$ to 1.2 : 1, submicron spheres assembled by nanoparticles and also attached with a few tiny nanoparticles on the surface (Fig. 2(c)) were obtained, quite like the chinar's fruit

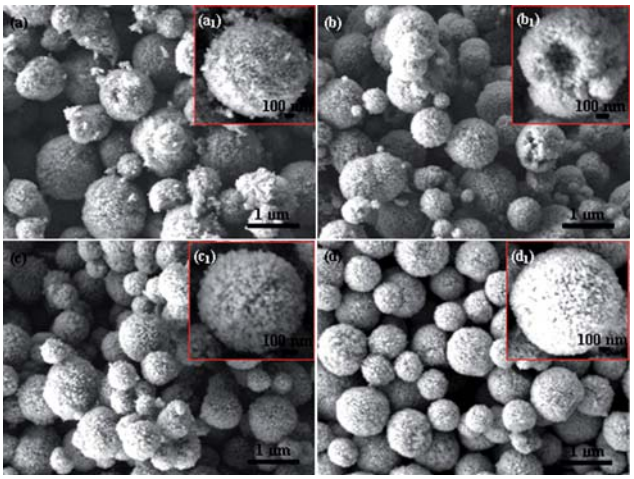

Fig. 2 Influences of the molar ratio of $MgCl_2$ (additive) and $SrCl_2$ (reactant) to Na_2CO_3 on the morphology of the hydrothermally treated submicron $SrCO_3$ spheres. *T*/°C: 190; time (h): 12.0; EDTA disodium salt : $Na_2CO_3 = 5 : 100$; (a,a_1) $MgCl_2 : Na_2CO_3 = 2.5 : 100$, $SrCl_2 : Na_2CO_3 = 1.05 : 1$; (b,$b_1$) $MgCl_2 : Na_2CO_3 = 5 : 100$, $SrCl_2 : Na_2CO_3 = 1.05 : 1$; (c,$c_1$) $MgCl_2 : Na_2CO_3 = 5 : 100$, $SrCl_2 : Na_2CO_3 = 1.2 : 1$; (d,$d_1$) $MgCl_2 : Na_2CO_3 = 5 : 100$, $SrCl_2 : Na_2CO_3 = 1.1 : 1$.

(Fig. 2(c_1)). Both the relatively broad distribution of the diameter of the spheres and some tiny nanoparticles attached on the sphere's surface implied the necessity for the further improvement of the uniformity of the spherical morphology. Keeping $MgCl_2 : Na_2CO_3$ as 5 : 100 and modifying $SrCl_2 : Na_2CO_3$ to 1.1 : 1, uniform hierarchical $SrCO_3$ submicron spheres with a relatively narrow distribution of the diameter of the spheres and no excessive distinct tiny nanoparticles attached on the sphere's surface were ultimately acquired (Fig. 2(d)), very like the plump and tight chinar's fruit (Fig. 2(d_1)). Statistical data demonstrated that approx. 95% of the hierarchical $SrCO_3$ submicron spheres had a diameter within the range of 600 nm to 1100 nm (Fig. S2),† and the diameter distribution was narrower than that of the mesoporous $SrCO_3$ spheres obtained in room temperature ILs, which contained two types of spheres (one type has diameters of 300–400 nm and the other type has diameters of 60–100 nm).[38]

On the other hand, keeping other conditions identical with those for the uniform submicron $SrCO_3$ spheres (Fig. 2(d–d_1)), irregular $SrCO_3$ particles with a wide size distribution and specific facets were formed after the hydrothermal treatment when without any additives (Fig. S3(a)),† or just with EDTA disodium salt and without $MgCl_2$ (Fig. S3(b)),† or only with CTAB (Fig. S3(d))†, which had been employed in the microemulsion-mediated solvothermal synthesis of $SrCO_3$ nanostructures including spheroids.[35] In contrast, the sole presence of $MgCl_2$ favored the formation of short $SrCO_3$ 1D assemblies (Fig. S3(c)),† additional presence of EDTA disodium salt promoted the formation of bouquet-like $SrCO_3$ architectures consisted of 1D nanostructures (Fig. 1(b_1)), and hydrothermal treatment propelled the ionization of EDTA disodium salt and further conversion from bouquet-like to spherical $SrCO_3$ architectures, *i.e.* submicron spheres. Presumably, Mg^{2+} ions might be absorbed onto specific surfaces of $SrCO_3$ *via* some weak interaction and thus favored the corresponding 1D growth during the hydrothermal treatment, and the absorbed Mg^{2+} ions were ultimately removed by subsequent thorough filtration and washing after the hydrothermal treatment. The pure phase of $SrCO_3$ was obtained in the final product, without distinct shift of the diffraction peaks observed (Fig. 1(c)), moreover, no magnesium element was detected in the EDS spectrum of the $SrCO_3$ submicron spheres (Fig. 3(b)), indicating no Mg^{2+} ions incorporated in $SrCO_3$. It was worth noting that in our case, the coexistence of $MgCl_2$ and EDTA disodium salt was required for the hydrothermal formation of present hierarchical $SrCO_3$ submicron spheres. In other words, the additives $MgCl_2$ and EDTA disodium salt played a synergistic effect during the formation of the present hierarchical $SrCO_3$ structures, which however needed further understanding.

3.3 Mesoporous structure determination of hierarchical $SrCO_3$ submicron spheres

TEM images of the hierarchical submicron $SrCO_3$ spheres (Fig. 2(d–d_1)) supported on the holey carbon film (Fig. 3(a)) revealed the spherical uniformity of the submicron spheres, and the corresponding EDS spectrum recorded from the focused area of the spheres hanging within the hole of the holey carbon film (Fig. 3(b)) definitely indicated that the submicron spheres comprised Sr, C and O, taking into consideration the background element Cu from the employed copper grid for supporting the holey carbon film. Notably, small spheres aggregated by small nanoparticles were also existed. A closer observation under a higher magnification on the sphere (Fig. 3(c)) clearly showed

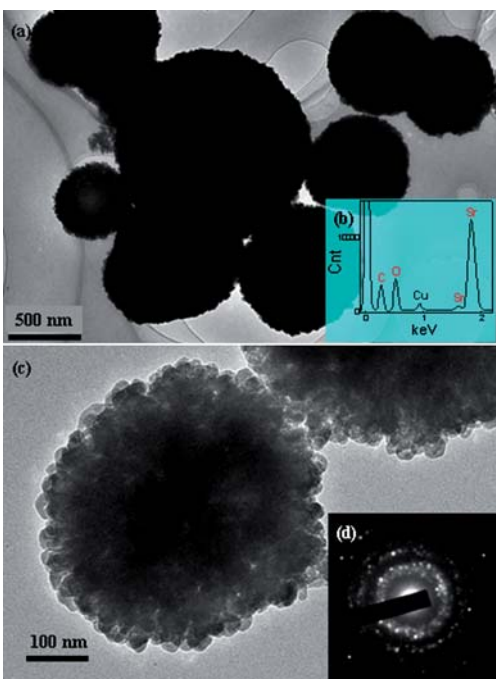

Fig. 3 TEM images of the hierarchical mesoporous $SrCO_3$ submicron spheres deposited onto the holey carbon film (a) and ordinary carbon film (c), supported by a copper grid, with the corresponding EDS spectrum (b) and SAED pattern (d) inserted. $SrCl_2 : Na_2CO_3 = 1.1 : 1$; EDTA disodium salt : $Na_2CO_3 = 5 : 100$; $MgCl_2 : Na_2CO_3 = 5 : 100$; *T*/°C: 190; time (h): 12.0.

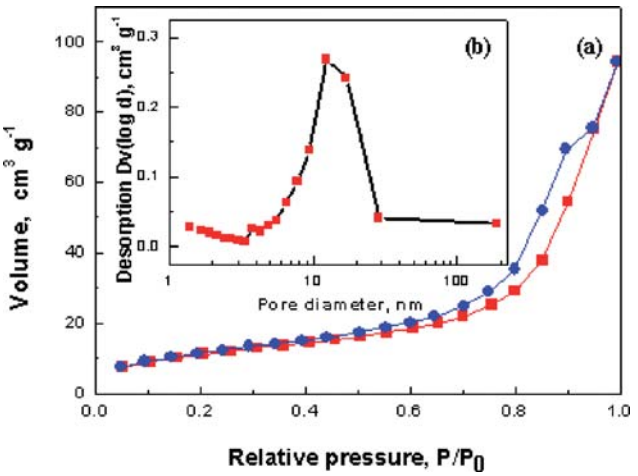

Fig. 4 Nitrogen adsorption–desorption isotherms (a) and pore size distribution (b) of the hierarchical mesoporous $SrCO_3$ submicron spheres. $SrCl_2 : Na_2CO_3 = 1.1 : 1$; EDTA disodium salt:$Na_2CO_3 = 5 : 100$; $MgCl_2 : Na_2CO_3 = 5 : 100$; *T*/°C: 190; time (h): 12.0.

that the submicron sphere was aggregated by multitudinal small nanoparticles (diameter: 20–40 nm), and the assembly even left some detective pores with a diameter of approx. 10 nm not only on or near the surface but also within the inner of the sphere. Meanwhile, the recorded SAED pattern (Fig. 3(d)) exerted some blur diffraction rings constituted of diffraction spots, which re-confirmed the crystalline structure of the submicron spheres and thus agreed with the previous XRD results (Fig. 1(c)). The nanocrystals existing within the submicron spheres, revealed by the polycrystalline characteristic SAED pattern and also small spherical aggregates (Fig. 3(a,c)), prefigured the probable assembling behavior of small nanoparticles in course of the formation of the hierarchical submicron $SrCO_3$ spheres.

N_2 adsorption–desorption isotherms were performed to fully evaluate the porous structures of the hierarchical submicron $SrCO_3$ spheres, as shown in Fig. 4. The N_2 adsorption–desorption isotherms (Fig. 4(a)) of the submicron spheres displayed type IV with an H3-type hysteresis loop at a high relative pressure, which indicated the hierarchical submicron spheres of mesoporous structure containing dominant slit pores and channels with a relatively uniform shape and size. Meanwhile, the multi-point BET results showed that the submicron spheres exhibited a specific surface area of 40.2 $m^2\ g^{-1}$ and a total pore volume of 0.145 $cm^3\ g^{-1}$. The specific surface area of the present submicron spheres is smaller than that of the mesoporous $SrCO_3$ spheres derived from room temperature ILs,[38] due to the relatively larger diameter of the present hierarchical mesoporous submicron spheres compactly aggregated by small nanoparticles. The relatively low surface area for mesoporous materials is attributed to the corresponding high density of $SrCO_3$ submicron spheres (Fig. 2(d-d_1)), since the metal oxides, especially multi-component metal oxides, tends to have a high density.[6,40] Nevertheless, the specific surface area and pore volume of the present mesoporous $SrCO_3$ submicron spheres are much larger than those of the hydrothermally synthesized mesoporous $InVO_4$ hierarchical microspheres (18.4 $m^2\ g^{-1}$, 0.057 $cm^3\ g^{-1}$).[6] The corresponding BJH desorption pore size distribution curve (Fig. 4(b)) showed that the hierarchical mesoporous $SrCO_3$ submicron spheres had a narrow pore size distribution, concentrating on 3–20 nm with an average pore diameter of 14.4 nm, in agreement with that derived from the TEM observation (Fig. 3(c)). The present average diameter is much larger than that of the mesoporous $SrCO_3$ spheres acquired in room temperature ILs (5.7 nm),[38] and the pore size distribution is much narrower compared with that of the mesoporous $InVO_4$ hierarchical microspheres.[6] Moreover, compared with those obtained in room temperature ILs, the present hydrothermally synthesized

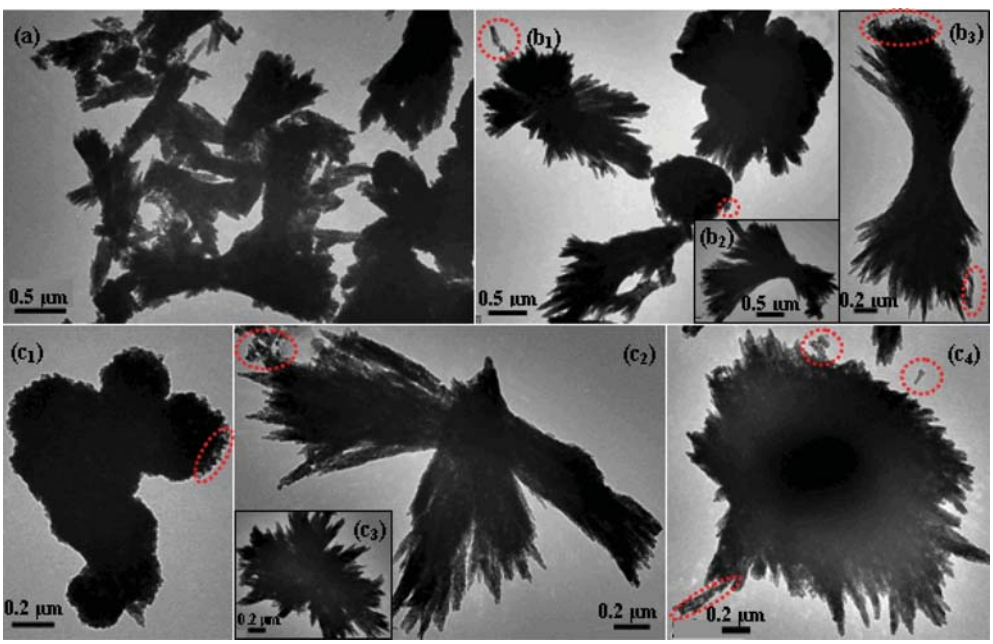

Fig. 5 Self-assembly behavior of the $SrCO_3$ nanoparticles obtained from the precipitate when heated to various temperature moments in course of the hydrothermal treatment. $SrCl_2 : Na_2CO_3 = 1.1 : 1$; EDTA disodium salt : $Na_2CO_3 = 5 : 100$; $MgCl_2 : Na_2CO_3 = 5 : 100$; *T*/°C: (a) 80; ($b_1$-$b_3$) 150; ($c_1$-$c_4$) 190.

mesoporous $SrCO_3$ submicron spheres (190 °C, 12.0 h) bear higher hydrothermal stability, indicating greater potentials as supports for catalysts.

3.4 Self-assembly behavior of $SrCO_3$ nanoparticles under hydrothermal treatment

Fig. 5 shows the self-aggregation, or self-assembly behavior of the $SrCO_3$ nanoparticles obtained from the precipitate when heated to various temperature moments in course of the hydrothermal treatment. When the precipitate at room temperature (Fig. 1(b,b_1)) was heated to 80 °C, more bouquet-like and even bouquet–bouquet attached (in a bundle-to-bundle headed manner) architectures were observed (Fig. 5(a)), promoted by the hydrothermal treatment, resembling the V-shape half-sheaf Bi_2S_3 nanostructures acquired from reaction of bismuth acetate-oleic acid complex with element sulfur in 1-octadecence.[41] As the temperature went up to 150 °C, two or three or more bouquet-like architectures tended to be attached each other in the bundles' ends (Fig. 5(b_1–b_3)), resulting more bouquet–bouquet attached architectures such as dumbbell-like (Fig. 5(b_3)), branched dumbbell- like (Fig. 5(b_2)) and even some rudimentary spherical structures (Fig. 5(b_1)), analogous to the dumbbell-like and dandelion-like $SrCO_3$ hierarchical architectures.[39] With temperature increased to 190 °C, quasi-spherical structures were observed, accompanied by general bouquet-bouquet attached architectures (Fig. 5(c_1–c_4)). It was worth noting that, as the increase in the hydrothermal temperature, tiny dissociative nanoparticles were inclined to be captured and thus absorbed or attached on the surfaces of the bouquet–bouquet attached architectures and spherical structures, as denoted by the red dotted line circle (Fig. 5(b_1,b_3,c_1,c_2,c_4)). The assembly and evolution of the bouquet-like nanostructures might readily arose the dominant slit pores and channels within the ultimate resultant hierarchical mesoporous $SrCO_3$ submicron spheres, in accordance with the information derived from the aforementioned N_2 adsorption–desorption isotherms (Fig. (4a)).

Aggregate behavior of the nanoparticles attached to the mesoporous $SrCO_3$ submicron spheres under the irradiation of the electron beam was recorded so as to further probe the formation of the present hierarchical mesoporous structures, as shown in Fig. 6. Under a high magnification TEM observation (Fig. 6(a)), the hierarchical submicron spheres were attached by tiny nanoparticles on the surfaces, contributing to the relatively rough spherical surfaces. Corresponded with the red dotted-line rectangular region (Fig. 6(a)), several nanoparticles assembled into a cross-hands profile were selected and then focused with the electron beam (Fig. 6(b)). With the irradiation time went on, the focused nanoparticles began to bend over and incline to the surface of the submicron sphere (Fig. 6(c)). Gradually, the nanoparticles inclined nearer and nearer to the submicron sphere (Fig. 6(d)), and finally embedded into the submicron sphere (Fig. 6(e)). Corresponding to the blue dashed-line rectangular region of the submicron sphere surface, there interplanar spacings of 0.337 nm detected from the legible lattice fringes (Fig. 6(e_1)), quite analogous to that of the (021) planes for the stand orthorhombic $SrCO_3$. After irradiated by the electron beam for some long time, the submicron sphere got a relatively smooth surface, especially on the red dotted-line rectangular region which had just experienced the former aggregation of the attached nanoparticles (Fig. 6(f)). The hydrothermal treatment, which supplied a relatively high temperature, high pressure and also solution environment, accordingly promoted the attachment of the swimming dissociative tiny nanoparticles onto the surfaces and also the final embedment of the nanoparticles into the submicron spheres. Furthermore, the fact that nanoparticles attached to the submicron spheres bent over, then inclined to and eventually embedded into the mesoporous $SrCO_3$ submicron spheres under the irradiation of the electron beam was believed to be helpful to in depth understand the hydrothermal formation of the hierarchical mesoporous spherical architectures, in that how quasi-sphere and rough-surface spheres evolved into relatively smooth-surface spheres.

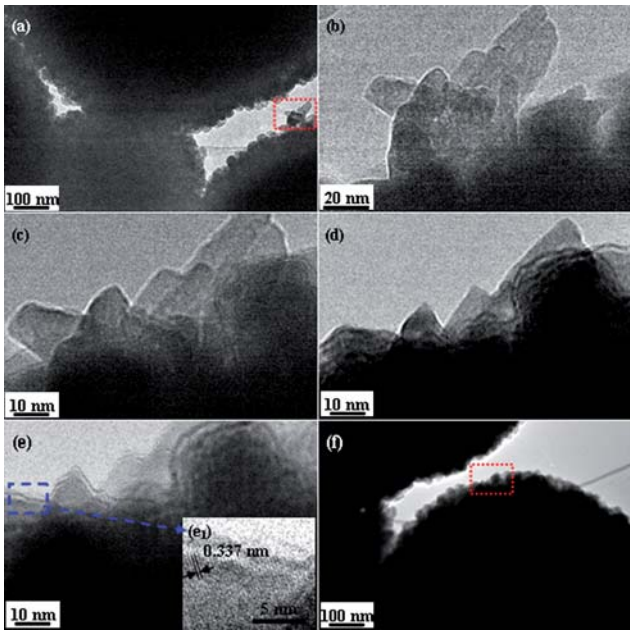

Fig. 6 Aggregate behavior of the nanoparticles attached to the hierarchical mesoporous $SrCO_3$ submicron spheres ($SrCl_2$: Na_2CO_3 = 1.1 : 1, EDTA disodium salt:Na_2CO_3 = 5 : 100; $MgCl_2$: Na_2CO_3 = 5 : 100, 190 °C; 12.0 h) under the irradiation of the electron beam. (a) The nanoparticles attached to a submicron sphere with relatively rough surface were selected, as shown by the red dotted-line rectangular region; (b) focused image of the selected nanoparticles recorded by a closer observation under a higher magnification; (c) the nanoparticles bent over and inclined to the submicron sphere; (d) the nanoparticles further inclined to the submicron sphere; (e) the nanoparticles ultimately embedded into the submicron sphere, with the interplanar spacings of 0.337 nm detected from the legible lattice fringes (e_1) corresponding to the blue dashed-line rectangular region of the submicron sphere surface; (f) the submicron sphere irradiated by the electron beam for some long time, with relatively smooth surface especially on the red dotted-line rectangular region which had just experienced the former aggregation of the attached nanoparticles.

3.5 Formation mechanism of hierarchical mesoporous $SrCO_3$ submicron spheres

The self-assembly behavior of $SrCO_3$ nanoparticles or morphology evolution of the present $SrCO_3$ submicron spheres

was by and large similar to the formation of hierarchical $SrCO_3$ architectures controlled by the "rod-to-dumbbell-to sphere" transformation[39] *via* room temperature aging. And such transformation phenomenon has also been found existed in the crystal growth of other material systems, including carbonates ($CaCO_3$, $BaCO_3$, $MnCO_3$, $CdCO_3$, *etc.*),[42–44] fluoroapatites ($Ca_5(PO_4)_3OH$),[45] and so on. Du *et al.*[38] explained the formation of the as-synthesized mesoporous $SrCO_3$ spheres in ILs *via* the reaction-limited aggregation (RLA), where only small fraction of the collisions result in the two particles involved adhering to each other. Similarly, in our case, the hydrothermal treatment of coprecipitated $SrCO_3$ at room temperature in presence of $MgCl_2$ and EDTA disodium salt could favor the RLA of the $SrCO_3$ nanocrystals *via* specific facets, probably resulted from minimizing interface energy, explaining the high structural stability of the aggregates. Resembling the oriented attachment (OA),[46–48] the RLA was believed to have controlled the original assembly of the nanoparticles in a head-to-head attached manner, in absence of any additives, into the rough bouquet-like $SrCO_3$ nanostructures containing 1D subassemblies (Fig. 1(a_1)) at room temperature, coincided with the OA existed in the microwave synthesis of branch-like $SrCO_3$ nanostructures.[37c] Meanwhile, the additives might act as the capping ligands and selectively adsorb onto the surfaces of nanocrystals, leading the oriented self-assembly of $SrCO_3$ nanocrystals to form smooth-surface bouquet-like $SrCO_3$ nanostructures (Fig. 1(b_1)) which further evolved into hierarchical mesoporous $SrCO_3$ submicron spheres under appropriate hydrothermal conditions.

Based on our experiments (Fig. 1, 5 and 6), the formation of the hierarchical mesoporous $SrCO_3$ submicron spheres from room temperature to hydrothermal treatment could be considered to have complied with RLA induced "rod-to-dumbbell-to-sphere" mechanism. Firstly, in presence of $MgCl_2$ and EDTA disodium salt, dropping Na_2CO_3 into $SrCl_2$ with an appropriate molar ratio results in $SrCO_3$ nanocrystals, and RLA of the nanocrystals leads to the original 1D assemblies, and the coalescence of the 1D assemblies side by side or head to head brings rough bouquet-like (Fig. 1(a_1)) and further smooth bouquet-like (Fig. 1(b_1)) nanostructures at room temperature probably originated from minimizing the whole interface energy, which thereafter successively undergo V-shape half-sheaf like (Fig. 5(a)), dumbbell-like (Fig. 5(b_3)), quasi-spherical or dandelion-like (Fig. 5(b_1,c_1–c_4)) nanostructures, and eventual hierarchical mesoporous $SrCO_3$ submicron spheres (Fig. 1(c_1), Fig. 2(d)) under appropriate hydrothermal conditions. Although the morphology evolution of the present $SrCO_3$ submicron spheres has indicated the conversion from rods to bouquets to dumbbells, which seems to some extent, analogous to the splitting crystal growth mechanism proposed by Tang and Alivisatos[41] and thereafter evidenced by Wang *et al.* in explaining the room temperature synthesis of hierarchical $SrCO_3$ architectures,[39] the specific intrinsic reasons for the present conversion still needs to be better and further investigated. In our view, RLA or similar OA, rather than splitting crystal growth, may have dominated the fancy formation of the bouquets (or V-shape half-sheaf) and subsequent conversion from bouquets to dumbbells (Fig. 5(b_3)) and branched dumbbells (Fig. 5(b_2)) of $SrCO_3$ in the present case, taking the presence of additives and related adsorbing effect into consideration. And the side by side coalescence in the bouquet's profile or head to head attachment in the bouquet's bottom probably resembles the similar OA growth of $MgBO_2(OH)$ nanowhiskers in hydrothermal conditions,[49] thus in depth structural characterization on the corolla and bottom of the bouquet especially neck of the dumbbell, and also the future *in situ* or real time TEM studies will be of considerable interest.[41]

4. Conclusions

In summary, hierarchical mesoporous $SrCO_3$ submicron spheres were obtained by a facile and direct hydrothermal treatment (190 °C, 12.0 h) of the room temperature precipitate derived from Na_2CO_3 and $SrCl_2$ solution in presence of appropriate amount of $MgCl_2$ and EDTA disodium salt as additives. The N_2 adsorption–desorption isotherms and the multi-point BET results indicated the present hierarchical submicron spheres of definite mesoporous structures with a specific surface area of 40.2 $m^2\ g^{-1}$, a total pore volume of 0.145 $cm^3\ g^{-1}$, and a narrow pore size distribution concentrating on 3–20 nm with an average pore diameter of 14.4 nm, much larger than that of the literature reported mesoporous $SrCO_3$ spheres acquired in room temperature ILs (5.7 nm).[38] The hierarchical mesoporous submicron spheres were formed *via* a RLA induced "rod-to-dumbbell-to-sphere" self-assembly mechanism, in which Na_2CO_3 was dropped into $SrCl_2$ with a molar ratio of $SrCl_2 : Na_2CO_3 = 1.1 : 1$ first, leading to $SrCO_3$ nanocrystals in presence of $MgCl_2$ and EDTA disodium salt. Then RLA of the nanocrystals resulted in the original 1D assembled nanostructures, and the coalescence of the 1D assemblies side by side or head to head brought rough bouquet-like and further smooth bouquet-like (*i.e.* V-shape half-sheaf like) nanostructures at room temperature. Thereafter the bouquet-like nanostructures successively underwent dumbbell-like, dandelion-like nanostructures, and eventual hierarchical mesoporous $SrCO_3$ submicron spheres, under appropriate hydrothermal conditions (190 °C, 12.0 h). The present hydrothermally synthesized hierarchical mesoporous $SrCO_3$ submicron spheres would enlarge the potential applications of $SrCO_3$ structures in the hierarchical mesoporous materials family for the narrow pore size distribution with a relatively large average pore diameter and a probable high hydrothermal stability, moreover, the developed facile reaction-limited aggregation induced "rod-to-dumbbell-to-sphere" self-assembly route may be expected for the preparation of other carbonates and non-silica hierarchical mesostructured materials.

Acknowledgements

The authors thank Professor Xi Zhang at Department of Chemistry, Tsinghua University, China, Associate Professor Xuefeng Guo at Department of Chemistry, Nanjing University, Dr Heng Zhang at Department of Chemical Engineering, Qufu Normal University, China, the editor and also the reviewers for their constructive suggestions or helpful discussions for the great improvement of the work, and also appreciate Dr Mengqiang Zhao and Associate Professor Ling Hu at Beijing Key Laboratory of Green Reaction Engineering and Technology, Department of Chemical Engineering, Tsinghua University, China, for their great help in the TEM characterization.

References

1 A. P. Alivisatos, *Science*, 1996, **271**, 933.
2 Y. N. Xia, P. D. Yang, Y. G. Sun, Y. Y. Wu, B. Mayers, B. Gates, Y. D. Yin, F. Kim and Y. Q. Yan, *Adv. Mater.*, 2003, **15**, 353.
3 (*a*) P. D. Yang and C. M. Lieber, *Science*, 1996, **273**, 1836; (*b*) X. D. Wang, J. H. Song, J. Liu and Z. L. Wang, *Science*, 2007, **316**, 102; (*c*) Y. Qin, X. D. Wang and Z. L. Wang, *Nature*, 2008, **451**, 809; (*d*) Z. W. Pan, Z. R. Dai and Z. L. Wang, *Science*, 2001, **291**, 1947.
4 (*a*) M. Li, H. Schnablegger and S. Mann, *Nature*, 1999, **402**, 393; (*b*) H. Colfen and S. Mann, *Angew. Chem., Int. Ed.*, 2003, **42**, 2350; (*c*) D. F. Zhang, L. D. Sun, C. J. Jia, Z. G. Yan, L. P. You and C. H. Yan, *J. Am. Chem. Soc.*, 2005, **127**, 13492; (*d*) M. Aizawa, A. M. Cooper, M. Malac and J. M. Buriak, *Nano Lett.*, 2005, **5**, 815; (*e*) D. Wang and C. M. Lieber, *Nat. Mater.*, 2003, **2**, 355; (*f*) S. O. Cho, E. J. Lee, H. M. Lee, J. G. Kim and Y. J. Kim, *Adv. Mater.*, 2006, **18**, 60.
5 X. F. Gao and L. Jiang, *Nature*, 2004, **432**, 36.
6 Y. Li, M. Cao and L. Feng, *Langmuir*, 2009, **25**, 1705.
7 H. J. Fan, P. Werner and M. Zacharias, *Small*, 2006, **2**, 700.
8 C. T. Kresge, M. E. Leonowicz, W. J. Roth, J. C. Vartuli and J. S. Beck, *Nature*, 1992, **359**, 710.
9 F. Schüth and W. Schmidt, *Adv. Mater.*, 2002, **14**, 629.
10 A. Corma, *Chem. Rev.*, 1997, **97**, 2373.
11 B. J. Scott, G. Wirnsberger and G. D. Stucky, *Chem. Mater.*, 2001, **13**, 3140.
12 M. Vallet-Regi, A. Rámila, R. P. del Real and J. Pérez-Pariente, *Chem. Mater.*, 2001, **13**, 308.
13 M. Hartmann, *Chem. Mater.*, 2005, **17**, 4577.
14 A. Imhof and D. J. Pine, *Nature*, 1997, **389**, 948.
15 Judith E. G. J. Wijnhoven and Willem L. Vos, *Science*, 1998, **281**, 802.
16 Galo J. de, A. A. Soler-lllia, C. Sanchez, B. Lebeau and J. Patarin, *Chem. Rev.*, 2002, **102**, 4093.
17 B. Smarsly, D. Grosso, T. Brezesinski, N. Pinna, C. Boissiere, M. Antonietti and C. Sanchez, *Chem. Mater.*, 2004, **16**, 2948.
18 S. Fujihara, T. Maeda, H. Ohgi, E. Hosono, H. Imai and S. H. Kim, *Langmuir*, 2004, **20**, 6476.
19 H. Song, R. M. Rioux, J. D. Hoefelmeyer, R. Komor, K. Niesz, M. Grass, P. D. Yang and G. A. Somorjai, *J. Am. Chem. Soc.*, 2006, **128**, 3027.
20 L. Chen, T. Horiuchi, T. Mori and K. Maeda, *J. Phys. Chem. B*, 1999, **103**, 1216.
21 M. Broyer, S. Valange, J. P. Bellat, O. Bertrand, G. Weber and Z. Gabelica, *Langmuir*, 2002, **18**, 5083.
22 Z. Zhang, Y. Han, F. S. Xiao, S. Qiu, L. Zhu, R. Wang, Y. Yu, Z. Zhang, B. Zou, Y. Wang, H. Sun, D. Zhao and Y. Wei, *J. Am. Chem. Soc.*, 2001, **123**, 5014.
23 Y. Li, J. Shi, Z. Hua, H. Chen, M. Ruan and D. Yan, *Nano Lett.*, 2003, **3**, 609.
24 D. W. Lee, C. Y. Yu and K. H. Lee, *J. Phys. Chem. C*, 2008, **112**, 5136.
25 K. Cassiers, T. Linssen, M. Mathieu, M. Benjelloun, K. Schrijnemakers, P. Van Der Voort, P. Cool and E. F. Vansant, *Chem. Mater.*, 2002, **14**, 2317.
26 (*a*) J. Yuan, K. Laubernds, Q. Zhang and S. L. Suib, *J. Am. Chem. Soc.*, 2003, **125**, 4966; (*b*) J. Ba, J. Polleux, M. Antonietti and M. Niederberger, *Adv. Mater.*, 2005, **17**, 2509; (*c*) Y. Zhu, L. Zhang, F. M. Schappacher, R. Pöttgen, J. Shi and S. Kaskel, *J. Phys. Chem. C*, 2008, **112**, 8623; (*d*) D. Yang, S. Sun, H. Meng, J.-P. Dodelet and E. Sacher, *Chem. Mater.*, 2008, **20**, 4677.
27 (*a*) X. Wang and Y. Li, *Angew. Chem., Int. Ed.*, 2002, **41**, 4790; (*b*) X. Wang and Y. Li, *J. Am. Chem. Soc.*, 2002, **124**, 2880; (*c*) Y. Li, J. Zhuang, X. M. Sun, Z. X. Deng and Y. D. Li, *Mater. Chem. Phys.*, 2002, **76**, 119; (*d*) S. C. Shen, Q. Chen, P. S. Chow, G. H. Tan, X. T. Zeng, Z. Wang and Reginald B. H. Tan, *J. Phys. Chem. C*, 2007, **111**, 700; (*e*) M. G. Ma, Y. J. Zhu and Z. L. Xu, *Mater. Lett.*, 2007, **61**, 1812; (*f*) W. C. Zhu, Q. Zhang, L. Xiang, F. Wei, X. Sun, X. Piao and S. Zhu, *Cryst. Growth Des.*, 2008, **8**, 2938.
28 (*a*) X. Wang, J. Zhuang, Q. Peng and Y. Li, *Nature*, 2005, **437**, 121; (*b*) M. Yoshimura and K. Byrappa, *J. Mater. Sci.*, 2008, **43**, 2085.
29 (*a*) Y. Feng, W. Lu, L. Zhang, X. Bao, B. Yue, Y. Lv and X. Shang, *Cryst. Growth Des.*, 2008, **8**, 1426; (*b*) Y. Shao, J. Sun and L. Gao, *J. Phys. Chem. C*, 2009, **113**, 6566; (*c*) X. Shang, W. Lu, B. Yue, L. Zhang, J. Ni, Y. Lv and Y. Feng, *Cryst. Growth Des.*, 2009, **9**, 1415; (*d*) F. Cao, W. Shi, L. Zhao, S. Song, J. Yang, Y. Lei and H. Zhang, *J. Phys. Chem. C*, 2008, **112**, 17095; (*e*) R. Yu, L. Yan, P. Zheng, J. Chen and X. Xing, *J. Phys. Chem. C*, 2008, **112**, 19896; (*f*) Y. Li, J. Liu, X. Huang and G. Li, *Cryst. Growth Des.*, 2007, **7**, 1350; (*g*) D. B. Kuang, B. X. Lei, Y. P. Pan, X. Y. Yu and C. Y. Su, *J. Phys. Chem. C*, 2009, **113**, 5508.
30 (*a*) A. F. Zeller, *Chem. Technol.*, 1981, **19**, 762; (*b*) M. Erdemoğlu and M. Canbazoğlu, *Hydrometallurgy*, 1998, **49**, 135.
31 T. J. Bastow, *Chem. Phys. Lett.*, 2002, **354**, 156.
32 (*a*) J. J. Shi, J. J. Li, Y. F. Zhu, F. Wei and X. R. Zhang, *Anal. Chim. Acta*, 2002, **466**, 69; (*b*) K. Omata, N. Nukui, T. Hottai, Y. Showa and M. Yamada, *Catal. Commun.*, 2004, **5**, 755; (*c*) L. Wang and Y. F. Zhu, *J. Phys. Chem. B*, 2005, **109**, 5118.
33 (*a*) I. Sondi and E. Matijević, *Chem. Mater.*, 2003, **15**, 1322; (*b*) Q. Huang, L. Gao, Y. Cai and F. Aldinger, *Chem. Lett.*, 2004, **33**, 290; (*c*) G. S. Guo, F. B. Gu, Z. H. Wang and H. Y. Guo, *Chinese Chem. Lett.*, 2005, **16**, 1101.
34 (*a*) J. Küther, M. Bartz, R. Seshadri, G. B. M. Vaughan and W. Tremel, *J. Mater. Chem.*, 2001, **11**, 503; (*b*) D. Rautaray, A. Sanyal, S. D. Adyanthaya, A. Ahmad and M. Sastry, *Langmuir*, 2004, **20**, 6827; (*c*) L. Shi and F. Du, *Mater. Res. Bull.*, 2007, **42**, 1550.
35 M. Cao, X. Wu, X. He and C. Hu, *Langmuir*, 2005, **21**, 6093.
36 (*a*) S. Li, H. Zhang, J. Xu and D. Yang, *Mater. Lett.*, 2005, **59**, 420; (*b*) M. G. Ma and Y. J. Zhu, *J. Nanosci. Nanotechnol.*, 2007, **7**, 4552.
37 (*a*) J. Yu, H. Guo and B. Cheng, *J. Solid State Chem.*, 2006, **179**, 800; (*b*) M. X. Zhang, J. C. Huo, Y. S. Yu, C. P. Cui and Y. L. Lei, *Chinese J. Struct. Chem.*, 2008, **27**, 1223; (*c*) M. G. Ma and Y. J. Zhu, *Mater. Lett.*, 2008, **62**, 2512.
38 J. Du, Z. Liu, Z. Li, B. Han, Y. Huang and J. Zhang, *Microporous Mesoporous Mater.*, 2005, **83**, 145.
39 W. S. Wang, L. Zhen, C. Y. Xu, L. Yang and W. Z. Shao, *Cryst. Growth Des.*, 2008, **8**, 1734.
40 P. Nguyen, H. T. Ng, J. Kong, A. M. Cassell, R. Quinn, J. Li, J. Han, M. McNeil and M. Meyyappan, *Nano Lett.*, 2003, **3**, 925.
41 J. Tang and A. P. Alivisatos, *Nano Lett.*, 2006, **6**, 2701.
42 (*a*) H. Cölfen and M. Antonietti, *Angew. Chem., Int. Ed.*, 2005, **44**, 5576; (*b*) S. H. Yu and H. Cölfen, *J. Mater. Chem.*, 2004, **14**, 2124; (*c*) H. Cölfen and L. Qi, *Chem.–Eur. J.*, 2001, **7**, 106.
43 S. H. Yu, H. Cölfen and M. Antoniietti, *J. Phys. Chem. B*, 2003, **107**, 7396.
44 S. Raz, S. Weiner and L. Addadi, *Adv. Mater.*, 2000, **12**, 38.
45 R. Kniep and S. Busch, *Angew. Chem., Int. Ed. Engl.*, 1996, **35**, 2624.
46 X. Wang, J. B. Xu and N. Ke, *Appl. Phys. Lett.*, 2006, **88**, 223108.
47 Y. Zhou and M. Antonietti, *J. Am. Chem. Soc.*, 2003, **125**, 14960.
48 R. L. Penn and J. F. Banfield, *Geochim. Cosmochim. Acta*, 1999, **63**, 1549.
49 W. C. Zhu, S. L. Zhu and L. Xiang, *CrystEngComm*, 2009, **11**, 1910.

